Boundary-Layer Meteorol (2012) 143:309–336
DOI 10.1007/s10546-012-9695-8

ARTICLE

Turbulent Structures in a Pine Forest with a Deep and Sparse Trunk Space: Stand and Edge Regions

Sylvain Dupont · Mark R. Irvine · Jean-Marc Bonnefond · Eric Lamaud · Yves Brunet

Received: 17 June 2011 / Accepted: 6 January 2012 / Published online: 2 February 2012

Abstract Forested landscapes often exhibit large spatial variability in vertical and horizontal foliage distributions. This variability may affect canopy-atmosphere exchanges through its action on the development of turbulent structures. Here we investigate in neutral stratification the turbulent structures encountered in a maritime pine forest characterized by a high, dense foliated layer associated with a deep and sparse trunk space. Both stand and edge regions are considered. In situ measurements and the results of large-eddy simulations are used and analyzed together. In stand conditions, far from the edge, canopy-top structures appear strongly damped by the dense crown layer. Turbulent wind fluctuations within the trunk space, where the momentum flux vanishes, are closely related to these canopy-top structures through pressure diffusion. Consequently, autocorrelation and spectral analyses are not quite appropriate to characterize the vertical scale of coherent structures in this type of canopy, as pressure diffusion enhances the actual scale of structures. At frequencies higher than those associated with canopy-top structures, wind fluctuations related to wake structures developing behind tree stems are observed within the trunk space. They manifest themselves in wind velocity spectra as secondary peaks in the inertial subrange region, confirming the hypothesis of spectral short-cuts in vegetation canopies. In the edge region specific turbulent structures develop just below the crown layer, in addition to canopy-top structures. They are generated by the wind shear induced by the sub-canopy wind jet that forms at the edge. These structures provide a momentum exchange mechanism similar to that observed at the canopy top but in the opposite direction and with a lower magnitude. They may develop as in plane mixing-layer flows, with some perturbations induced by canopy-top structures. Wake structures are also observed within the trunk space in the edge region.

Keywords Coherent eddy structures · Forest canopy · Large-eddy simulation · Plane mixing-layer flow · Trunk space · Wind spectra

S. Dupont (✉) · M. R. Irvine · J.-M. Bonnefond · E. Lamaud · Y. Brunet
INRA, UR1263 Ephyse, Villenave d'Ornon, France
e-mail: sdupont@bordeaux.inra.fr

1 Introduction

Forests play an important role in biosphere–atmosphere exchanges of momentum, energy and scalars such as water vapour and carbon dioxide. One of the difficulties involved in quantifying such exchanges arises from their large spatial variability. Vertically, forests are characterized by various distinct layers such as crown layer, trunk space and understorey, which specifically contribute to scalar exchanges (e.g., Black and Kelliher 1989; Lamaud et al. 1996, 2001; Constantin et al. 1999; Misson et al. 2007). Horizontally, forests are often fragmented due to the presence of clearings, roads, changes in height, etc. Such features induce local advection, particularly in edge regions, which should be accounted for when estimating forest-atmosphere exchanges (Klaassen et al. 2002; Sogachev et al. 2008).

It is well known that exchanges of momentum, heat and mass between canopies and the atmosphere are comprised for a substantial part by intermittent, energetic downward-moving gusts, caused by large coherent eddy structures scaling with canopy height (Gao et al. 1989; Lu and Fitzjarrald 1994; Finnigan 2000). On average they take the form of superposed hairpin vortices with strong 'sweeps' (gusts) and weak 'ejections' (bursts) between the hairpin legs (Finnigan et al. 2009). These structures are generated by processes similar to those occurring in plane mixing layers (Raupach et al. 1996). The development stages of coherent structures occur at random locations over homogeneous canopies, while they occur at relatively well-defined locations in the adjustment region after the leading edge (Dupont and Brunet 2009). Most of our knowledge on canopy coherent structures is mostly on canopies with a relatively uniform vertical (and horizontal) foliage distribution.

In a recent study (Dupont et al. 2011) the statistics of turbulent flow over a maritime pine forest, characterized by a dense crown layer and a deep, sparse trunk space, have been studied in stand and edge regions. It was shown that this particular foliage distribution induces some specific flow features, as compared to more uniform forests, which may result from, or induce, differences in coherent turbulent structures within the canopy. By 'uniform forest' we mean a forest with a homogeneous vertical foliage distribution. The goal of the present paper is to investigate in neutral stratification the turbulent structures within this forest, in both stand and edge regions. Only few studies have focussed on turbulent structures over such types of vertically discontinuous forest, and this was only done far from the edge (see, for example, Baldocchi and Meyers 1988a,b).

The main characteristics of the turbulent flow observed over a maritime pine forest in Dupont et al. (2011) are summarized in Fig. 1. Near the edge region (Fig. 1a) the turbulent region developing above the canopy starts closer to the edge than over more uniform forests. No well-defined enhanced gust zone is present upwind from the turbulent region, and turbulence intensity is slightly larger within the canopy. A strong wind jet can be seen in the sub-canopy, and a layer with positive momentum flux, just below the crown layer, starts forming at the edge (Fig. 1b). It may extend over a long distance if the turbulent vertical transport of downward shear stress from above is insufficient to compensate the upward shear stress induced by the sub-canopy wind jet. These edge-flow characteristics were observed to decay very slowly with increasing distance from the edge, so that the adjustment region is much longer than $10h$, h being the canopy height. Well within the stand, wind velocity is strongly reduced in magnitude by the action of the dense crown layer. It reaches a minimum in the lower part of the crown layer, then increases further down and reaches a secondary maximum within the trunk layer (Fig. 1b). Similarly, the turbulent kinetic energy (TKE) (not shown) and momentum flux rapidly decrease within the crown layer, then remain quasi-constant below the latter, with very small values for the momentum flux.

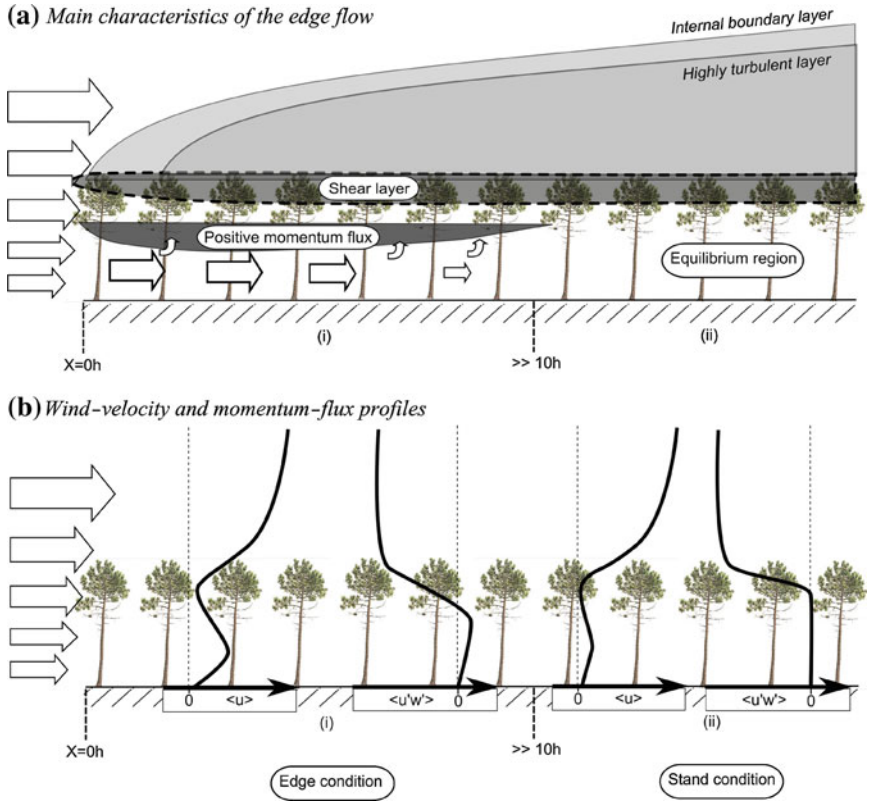

Fig. 1 Idealized representation of the main characteristics of stand and edge flows for a mature maritime pine forest characterized by a deep and sparse trunk space, and a mean height h. (**a**) is adapted from Dupont et al. (2011). The idealized representation of wind-velocity and momentum-flux profiles (**b**) is deduced from Dupont et al. (2011)

The unusual behaviour of the momentum-flux profiles in this particular forest, as sketched in Fig. 1b, raises several questions in terms of turbulent structures within forests with a deep trunk space. In stand regions firstly, does the near-zero value of the momentum flux in the trunk space imply that coherent eddy structures are unable to penetrate deeply into the canopy? In other words, is there a strong decoupling between the trunk space and the atmosphere above? Secondly, what does the positive momentum flux in the sub-canopy near the edge involve in terms of canopy coherent eddy structures? In order to address these issues, the turbulent structures associated with the momentum flux in this forest are investigated in stand and edge regions by using both in situ measurements and large-eddy simulation (LES). LES has appeared very helpful in understanding the general three-dimensional behaviour of the flow dynamics around measurement points (Dupont et al. 2011). The first-order to the fourth-order moments derived from LES time series were validated over this forest by Dupont et al. (2011) in both stand and edge configurations. It was observed that the LES model simulates remarkably well most of the characteristics of the turbulent flow, including the momentum-flux profiles.

The present paper is structured as follows. The in situ and numerical experiment set-ups, as well as the statistical approaches used to characterize turbulent structures, are described

in Sect. 2. The results on turbulent structures, as deduced from quadrant, two-point autocorrelation and spectral analyses, are presented in Sect. 3. The characteristics of the turbulent structures developing in this particular forest are then discussed in Sect. 4, in both stand and edge regions, and finally we move to conclusions in Sect. 5.

2 Material and Methods

As the in situ and numerical experiments are fully described in Dupont et al. (2011), only an overview is presented here.

2.1 In Situ Experiment

The measurements used here were performed in the period 2006–2008 at Le Bray site (44°43′1.6″N, 0°46′9.5″W), a maritime pine (*Pinus pinaster* Ait.) forest plot located in the Les Landes region, south-western France. The forest was mature at the time of the experiment and its characteristics did not change significantly over the period. Mean tree height (h), tree density, leaf area index (LAI) and mean stem diameter at breast height were about 22 m, 410 trees ha^{-1}, 1.8 and 0.33 m, respectively. The forest plot was characterized by a dense crown layer located between 13 and 22 m, and a very sparse and open trunk space below 13 m. The mean vertical distribution of the frontal area density A_f is shown in Fig. 2b. The soil was covered with graminae approximately 0.7 m high with a $LAI = 1.5$.

Until 2000 this site had excellent homogeneity criteria, as required for the eddy-covariance method: the terrain was flat (slope less than 0.2° in all directions) and the site was surrounded by similar stands, with fetches longer than 1 km in the prevailing wind directions. Following the December 1999 Lothar windstorm, clearcuts were made at about 200 m ($9h$) to the north-west, one of the prevailing wind sectors, and 260 m ($12h$) south-west from the 40-m high tower, inducing possible edge effects on tower measurements in both sectors (see Fig. 2a). This allowed us to study stand and edge conditions from this single site, by splitting the data into different wind sectors.

During the whole period turbulence measurements were recorded continuously at 41.50 and 7.05 m, from two tri-axial sonic anemometers set up on the tower. A mean horizontal wind-velocity profile was also continuously measured using nine cup anemometers located on the tower between 11 and 32 m. In addition to these background measurements, two short-term experiments were specifically performed for this study:

- From April to September 2006 wind-velocity components and air temperature were measured at five heights within the canopy on a 13-m high mast erected at $4h$ from the north-western edge (Fig. 2a, c), using tri-axial sonic anemometers operating at 20 Hz. These heights (1.60, 4.40, 7.05, 9.00 and 11.15 m) were chosen so as to explore the entire trunk space, between the understorey and the crown layer. Except for the sonic at 9.00 m that was installed during four months only, all measurements were performed throughout the period.
- From April to November 2008 six tri-axial sonic anemometers were set up on the flux tower, in addition to the other two (Fig. 2b). Five levels were located within the trunk space (4.50, 7.05, 9.00, 11.50, 13.00 m), one was in the crown layer (17 m), one at canopy top (22 m), and one at about twice the canopy height (41.50 m). Measurements were performed during eight months at 20 Hz, except for the anemometers at 17 and 22 m, which were installed during one and five months only, respectively.

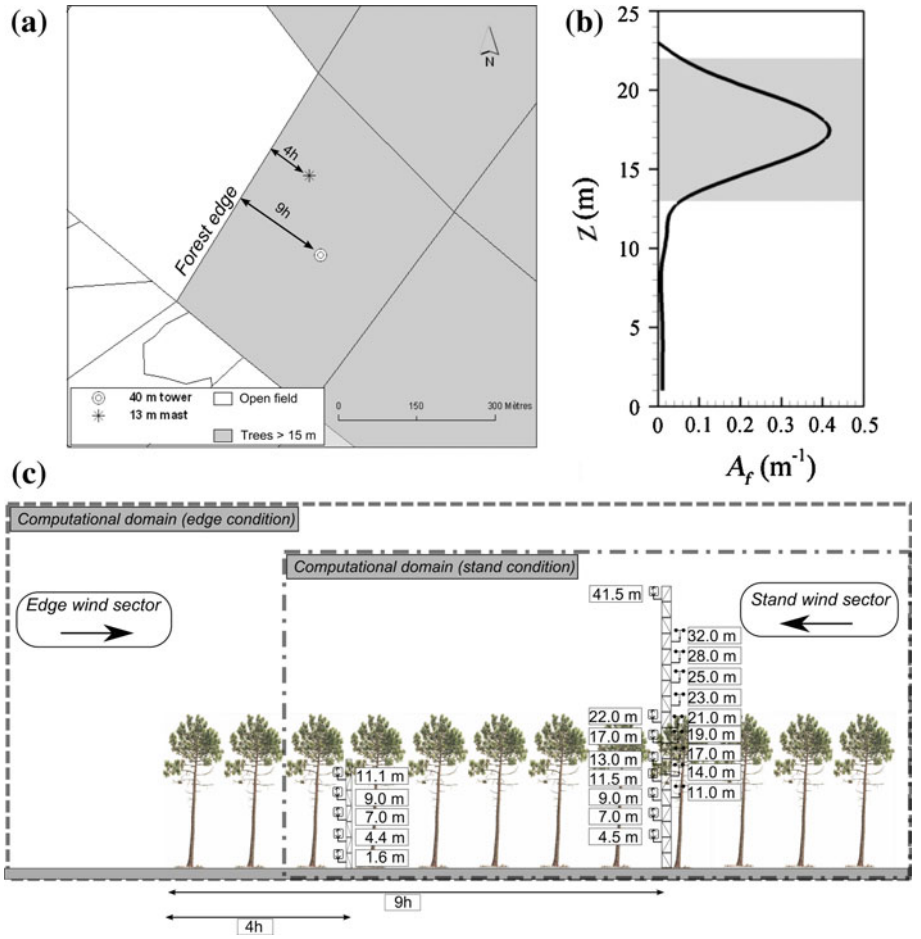

Fig. 2 **a** Map of the experimental site. **b** Vertical profile of the frontal area density of the maritime pine forest (A_f), with the *shaded area* representing the crown layer. **c** Streamwise cross-section of the experimental set-up for the two wind directions considered here. These wind directions define the heterogeneous (edge) and homogeneous (stand) cases, respectively, associated with two computational domains (*dashed* and *dash-dot lines*, respectively). The small mast erected at $4h$ downwind from the edge is equipped with five sonic anemometers and the tower located at $9h$ downwind from the edge is equipped with eight sonic anemometers and nine cup anemometers

The experimental layout is sketched in Fig. 2c and its technical characteristics are summarized in Table 1. All sonic anemometers were intercompared before and after the experiment.

The integration time for all statistics is taken as 30 min. Only near-neutral conditions are considered here, with a selection criterion defined as $-0.05 < h/L < 0.05$ (L being the Obukhov length estimated from the top-level sonic anemometer). At all heights the wind-velocity components are rotated horizontally so that u represents the horizontal component along the mean wind direction x and v the horizontal component along the transverse direction y. In order to account for possible errors in the vertical orientation of the sonic anemometers and provide the actual vertical component w, a second rotation is performed at each height around the y-axis, on a monthly basis. As the streamlines are not necessarily

Table 1 Characteristics of the experiments

Year	$x = 4h$				$x = 9h$					
	Sonic heights (m)	Type of sonic anemometer	Sampling freq. (Hz)	Number of runs for sonics (edge-stand)	Cup anemometer heights (m)	Sonic heights (m)	Type of sonic anemometer	Sampling freq. (Hz)	Number of runs for sonics (edge-stand)	Number of runs for cups (edge-stand)
2006	11.15	RM Young 81000V[a]	20	184–239	32.00	41.50	RM Young 81000V[a]	20	308–446	
	09.00	Gill R3[b]	20	147–148	28.00	07.05	RM Young 81000V[a]	20	299–425	
	07.05	RM Young 81000V[a]	20	230–257	25.00					
	04.40	RM Young 81000V[a]	20	231–250	23.00					
	01.60	RM Young 81000V[a]	20	175–180	21.00					
					19.00					
					17.00					
					14.00					
					11.00					

Table 1 continued

Year	$x = 4h$				$x = 9h$					
	Sonic heights (m)	Type of sonic anemometer	Sampling freq. (Hz)	Number of runs for sonics (edge-stand)	Cup anemometer heights (m)	Sonic heights (m)	Type of sonic anemometer	Sampling freq. (Hz)	Number of runs for sonics (edge-stand)	Number of runs for cups (edge-stand)
2008					32.00	41.50	RM Young 81000V[a]	20	181–166	169–161
					28.00	22.00	Gill R3[b]	20	123–116	179–166
					25.00	17.00	RM Young 81000V[a]	20	10–45	181–166
					23.00	13.00	RM Young 81000V[a]	20	121–115	181–166
					21.00	11.50	RM Young 81000V[a]	20	141–152	181–165
					19.00	09.00	RM Young 81000V[a]	20	135–153	96–95
					17.00	07.05	Gill R3[b]	20	172–157	180–166
					14.00	04.50	Gill R3[b]	20	155–154	141–150
					11.00					180–166

[a] R.M. Young Company, Traverse City, Michigan, USA
[b] Gill Instruments, Lymington, Hampshire, UK

horizontal in the edge sector, the monthly rotational angles are calculated from the measurements performed in the stand sector, and subsequently applied to all the samples.

The averaging procedure is only performed over time for the measurements while it is also performed over space for the simulations (see next section). Both averaging procedures are equivalent if dispersive fluxes, resulting from spatial correlations of time-averaged quantities, vanish (Raupach and Shaw 1982). As reviewed by Poggi and Katul (2008), in situ and wind-tunnel measurements have shown that dispersive fluxes are negligible in dense canopies (Raupach et al. 1986; Cheng and Castro 2002) while they can be significant (i.e. of the same order as mean fluxes) in the lower layer of sparse canopies (Bohm et al. 2000; Christen and Vogt 2004; Poggi et al. 2004). Our canopy may be considered as intermediate between these two cases ($LAI = 1.8$). However, since statistical variables were also ensemble-averaged over a relative large range of wind directions (60° and 120° ranges for edge and stand cases, respectively), we believe that possible local horizontal inhomogeneity effects on the measurements should then be removed. Consequently, dispersive fluxes may be neglected.

The number of available 30-min samples left after standard quality control (see Dupont et al. 2011) is given in Table 1 for each sonic and cup anemometer.

2.2 Numerical Experiment

The Advanced Regional Prediction System (ARPS) version 5.1.5 (Xue et al. 2000, 2001), developed at the Center for Analysis and Prediction of Storms (CAPS) at the University of Oklahoma, U.S.A. is used in this study in order to simulate turbulent wind flow above and within the forest canopy. ARPS was modified by Dupont and Brunet (2008c) so that the model could be applied in LES mode at canopy scale. This consisted in implementing, (i) a pressure and viscous drag force term in the momentum equation shown in the Appendix (Eq. 4), and (ii) a sink term in the equation for subgrid-scale (SGS) TKE, representing the acceleration of the dissipation of turbulent eddies in the inertial subrange. The simulated mean statistics, as well as the development of coherent structures, were successfully validated against field and wind-tunnel measurements in several canopy configurations with relatively uniform vertical foliage distributions: homogeneous canopy on a flat terrain (Dupont and Brunet 2008c), forest-clearing-forest pattern (Dupont and Brunet 2008a,b, 2009), forested hill (Dupont et al. 2008), and waving crop (Dupont et al. 2010).

In Dupont et al. (2011) the statistical fields simulated by this new version of ARPS over the maritime pine forest studied here were also successfully validated in both stand and edge regions. We use here the same three-dimensional simulations in order to characterize the turbulent structures above and within this forest canopy. Two simulations were performed: one over a homogeneous canopy representing the stand-wind sector configuration, hereafter referred to as the stand case, and one over a forest-clearing-forest pattern representing the edge-wind sector configuration, referred to as the edge case. In the stand case the domain extends over $400 \times 200 \times 200$ m^3, corresponding to $200 \times 100 \times 130$ grid points in the x (streamwise), y (spanwise) and z (vertical) directions respectively. In the edge case the domain size is $690 \times 200 \times 200$ m^3, with $345 \times 100 \times 130$ grid points. In both cases the grid resolution is 2 m in the horizontal, and 1 m in the vertical below $z = 84$ m; above this level the grid is stretched. The 2006–2008 Le Bray site characteristics are used to define the canopy parameters (Table 1; Fig. 2b). Forest height h is set to 22 m and the frontal area density profile A_f of the canopy is that shown in Fig. 2b. The drag coefficient C_d is assumed constant within the canopy and equal to 0.26, as was evaluated by Sellier et al. (2008) at this site. In the edge case the clearing length is set to $20h$, as a compromise between the available computational time and a clearing size large enough to limit the effect of the upwind forest

on the edge flow (see Fig. 7 in Dupont et al. (2011)). In fact the presence of a far upwind forest in the simulations is expected to be more representative of the present experimental site than an idealized semi-infinite clearing-forest transition.

The lateral boundary conditions are periodic and the bottom boundary is considered as rigid. The surface momentum flux is parametrized using a bulk aerodynamic drag law. A 70-m deep Rayleigh damping layer is used at the upper boundary in order to absorb upward-propagating wave disturbances and eliminate wave reflection. The flow is driven by a pressure gradient associated with the geostrophic wind. The velocity fields are initialized by a meteorological pre-processor (Pénelon et al. 2001) with uniform potential temperature and a dry atmosphere.

After the flow has reached equilibrium all statistical fields are computed using a space and time averaging procedure. At each z position space averaging is performed over all x and y locations in the stand case and only over all y locations in the edge case. Time averaging is performed over 90 instantaneous samples collected every 20 s during a 30-min period. Consequently, wind-velocity components u_i can be decomposed as $u_i = \langle u_i \rangle + u_i'$ where the angular brackets define the time and space average, and the prime the deviation from the averaged value.

2.3 Turbulent Structure Analysis

Coherent eddy structures over vegetation canopies have been investigated for years from in situ, wind-tunnel and numerical experiments (see Finnigan 2000, for a review). A range of tools has been used for this purpose such as wind-velocity spectra, conditional analyses (e.g., quadrant analysis, wavelet transform), space-time velocity correlations (Shaw et al. 1995; Su et al. 2000; Dupont and Brunet 2009), empirical orthogonal functions (Finnigan and Shaw 2000), or ensemble averaging from LES (Finnigan et al. 2009). We use here a combination of three complementary techniques.

Firstly, a quadrant analysis is performed on measured and simulated velocity time series in order to assess the type of eddy motions responsible for momentum transfer in the canopy. Eddy motions are split up into four quadrants, irrespective of their duration:

- Quadrant I: $u' > 0$ and $w' > 0$ (outward interaction)
- Quadrant II: $u' < 0$ and $w' > 0$ (ejection)
- Quadrant III: $u' < 0$ and $w' < 0$ (inward interaction)
- Quadrant IV: $u' > 0$ and $w' < 0$ (sweep).

The momentum flux $\langle u'w' \rangle_S$ induced by extreme events, where S is a threshold value characterizing events such as $|u'w'| > S\,|\langle u'w' \rangle|$, is decomposed into:

$$\langle u'w' \rangle_S = \langle u'w' \rangle_{\mathrm{I}S} + \langle u'w' \rangle_{\mathrm{II}S} + \langle u'w' \rangle_{\mathrm{III}S} + \langle u'w' \rangle_{\mathrm{IV}S} \tag{1}$$

where $\langle u'w' \rangle_{\mathrm{I}S}$, $\langle u'w' \rangle_{\mathrm{II}S}$, $\langle u'w' \rangle_{\mathrm{III}S}$, and $\langle u'w' \rangle_{\mathrm{IV}S}$ are the magnitudes of the momentum flux in quadrants I, II, III and IV, respectively. Similarly, the number of events responsible for extreme momentum fluxes can be written as:

$$nb_S = nb_{\mathrm{I}S} + nb_{\mathrm{II}S} + nb_{\mathrm{III}S} + nb_{\mathrm{IV}S} \tag{2}$$

where $nb_{\mathrm{I}S}$, $nb_{\mathrm{II}S}$, $nb_{\mathrm{III}S}$, and $nb_{\mathrm{IV}S}$ are the number of events in quadrants I, II, III and IV, respectively, contributing to the momentum flux.

Secondly, a zero time-lag two-point autocorrelation analysis of the velocity components and pressure perturbation is performed on LES fields to characterize the mean size of coherent

eddy structures in each quadrant. The autocorrelation is defined as:

$$R_{\phi\phi}^{QS}(x - X, y, z) = \frac{\langle \phi(X, 0, Z)\phi(x, y, z)\rangle_{QS}}{\sqrt{\langle \phi'(X, 0, Z)^2\rangle_{QS}\langle \phi'(x, y, z)^2\rangle_{QS}}}, \quad (3)$$

where ϕ is either u, w or the pressure perturbation p, and Q is either I, II, III or IV. The reference point of the correlation is located at a given height Z, and at the origin of the horizontal axis ($X = 0$) in the stand case; in the edge case it is at distance X from the canopy leading edge. The quadrant associated with each eddy structure is deduced from the signs of u' and w' at the reference point of the correlation. Hence, the angular brackets in Eq. 3 denote a space-time average for each quadrant-type structure detected at the reference point.

Finally, a spectral analysis is performed on measured wind-velocity components in order to identifiy the most energetic turbulent structures. The number of 30-min samples used to average wind spectra is given in Table 1.

3 Results

3.1 Quadrant Analysis

Figure 3 shows the contribution of all four quadrants to the momentum flux (in magnitude and number of events), for overall ($S = 0$) and extreme events ($S = 3$), in both stand (a) and edge (b at $x = 4h$ and c at $x = 9h$) regions (see Eqs. 1 and 2). In this figure the measured values (symbols) are compared to those obtained from LES (lines), and the error bars represent the standard deviation of the measured quadrant fluxes. This figure allows one to determine the type of turbulent structures, characterized by the instantaneous values of u' and w', that are responsible for momentum transport, through the $u'w'$ magnitude and number.

As previously observed over vegetation canopies (Raupach et al. 1996; Finnigan 2000), above about two canopy heights the momentum-flux magnitude is equally controlled by sweeps (quadrant IV) and ejections (quadrant II), whereas around the canopy top, i.e. from the crown layer to about two canopy heights, it is dominated by sweep motions, and in the second place by ejection motions. This feature is verified in both stand and edge regions, as well as for all and extreme events. Around the canopy top, ejections are more frequent than sweeps when all events are considered, while sweeps become more frequent when only extreme events are considered. This distribution of the momentum flux between the four quadrants confirms previous findings that momentum transfer at the canopy top is primarily due to the occurrence of fast, downward-moving gusts (sweeps).

Below the crown layer, i.e. within the trunk space, in the stand sector the momentum flux appears equally distributed between the four quadrants, in all cases (magnitude and number of events; all and extreme events). This result may reflect the isotropy of turbulence in this region of the canopy where the variances of the three wind components are similar in magnitude (Dupont et al. 2011). In the edge case the quadrant structure of the momentum flux changes drastically just below the crown layer, where this flux takes positive values (Fig. 1b). When considering all events, slow downward-moving motions (quadrant III) become slightly dominant in magnitude, followed by fast upward-moving ones (quadrant I). The latter appear more frequent than the former. In the case of extreme events, these two motion types equally dominate in magnitude the momentum flux, while slow downward-moving motions are now more frequent than fast upward-moving ones. This distribution of events just below the crown

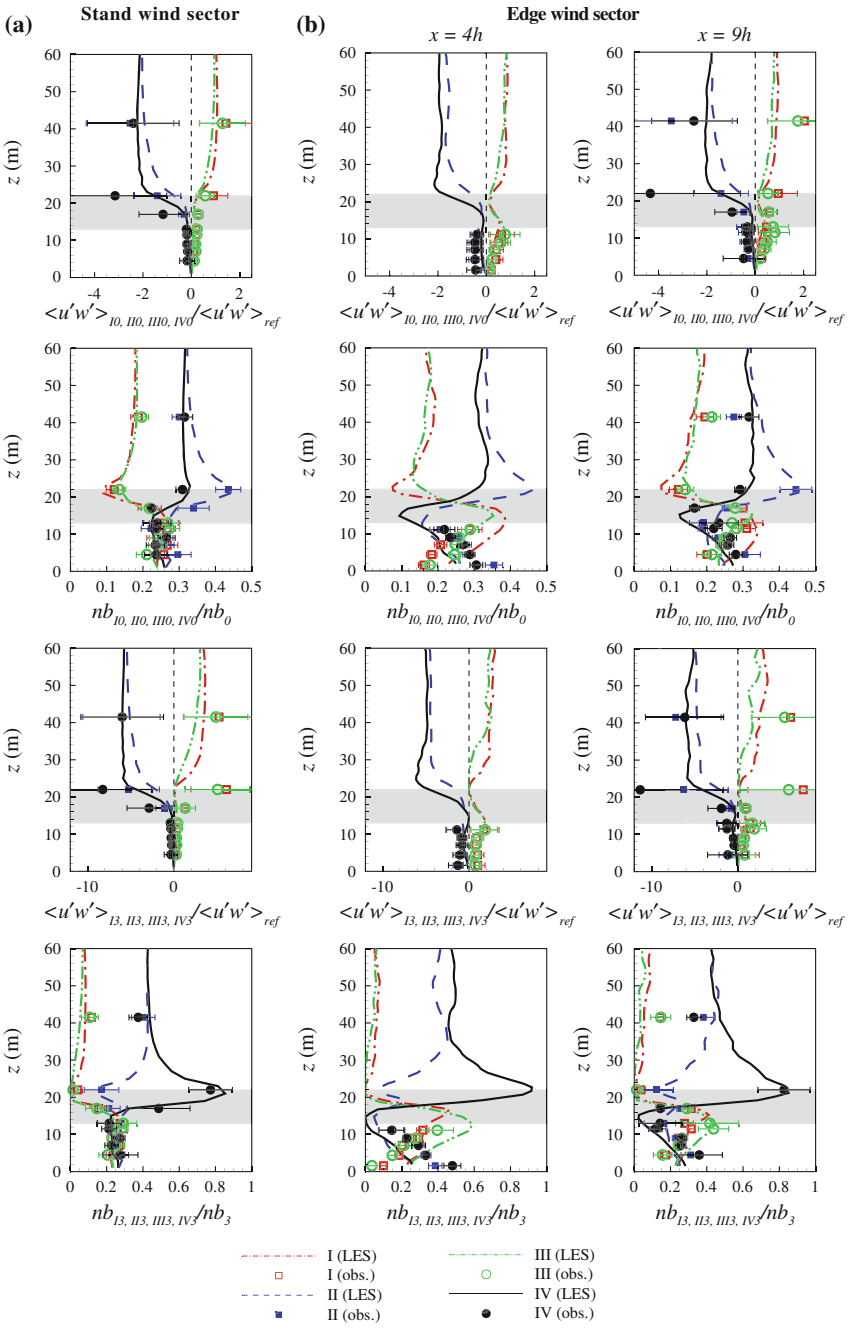

Fig. 3 Observed (*symbols*) and simulated (*lines*) contribution of the four quadrants to momentum flux in terms of magnitude ($\langle u'w' \rangle$) and event number (nb), for the stand (**a**) and the edge (**b**) wind sectors, and for all ($S = 0$) and extreme events ($S = 3$) (see Sect. 2.3 for more details). All quadrant momentum fluxes are normalized by the mean momentum flux $\langle u'w' \rangle_{\text{ref}}$ estimated at $x = 9h$ and $z = 41.50$ m (highest level of the tower). *Error bars* indicate the standard deviation of the corresponding variable. The *shaded area* represents the crown layer

layer is slightly more pronounced closer to the edge ($x = 4h$), where the positive values of the momentum flux are larger.

Close to the ground, as the momentum flux becomes negative, sweep and ejections tend to dominate again and become more frequent than the other two motion types. This is particularly visible at $x = 4h$ (Fig. 3b). These features are reminiscent of a surface layer, which can be expected in the lowest region of such an open canopy.

The slight canopy-top discrepancy visible in Fig. 3 between observation and simulation on the contribution of the four quadrants to momentum flux is probably related to a stability effect. As the selection criterion for neutral conditions is defined from the measurements at the highest level (41.50 m), non-neutral conditions may occur at lower levels during 'neutral' runs, especially during daytime and nighttime transitions. The larger error bars observed above the canopy than within the canopy are explained by the larger magnitude of the momentum flux above the canopy, along with a large temporal variability due to the fluxes being averaged over different wind conditions. Despite these occasional differences in magnitude, the behaviour of the momentum flux in the four quadrants appears fairly well reproduced by the model in both wind sectors. In summary, this quadrant analysis shows that, (i) in the stand region the near-zero value of the momentum flux in the trunk space results from an equilibrium between positive and negative fluctuations of $u'w'$, and (ii) near the edge a momentum exchange mechanism similar to that observed at the canopy top occurs below the crown layer but in the opposite vertical direction and with a much lower magnitude. This mechanism results in an upward momentum flux in this region of the flow. Quadrants I and III contribute to this positive momentum flux to a large extent, in a way similar to sweep and ejection motions associated with a mean downward momentum flux. We believe that this specific distribution of the momentum flux visible in the present canopy all along the region extending to at least $9h$ from the edge, and confirmed by LES, has never been reported before in the literature.

3.2 Simulated Spatial Correlations

After the types of turbulent structures associated with momentum transfer through the canopy have been identified, we now investigate from LES the mean size and shape of these structures in stand and edge regions. Figures 4a–c and 5a–c (stand) and Figs. 6a–c and 7a–c (edge, $x = 4h$) show the two-point autocorrelations R_{uu}, R_{ww} and R_{pp}, deduced from the LES (Eq. 3) for each quadrant, using a reference point either at canopy top ($z = 22$ m) or in the trunk space ($z = 6$ m). Autocorrelations at $x = 9h$ downwind from the edge are not shown as they only represent an intermediate case between stand and edge at $4h$. Composite average fields of wind-vector fluctuations and pressure perturbations associated with all events of each quadrant are also shown in Figs. 4d, 5d, 6d, and 7d. Note that in the latter figures the arrows have a uniform size and only show the direction of ensemble-averaged wind-vector fluctuations. As the main flow characteristics (Dupont et al. 2011) and the distribution of the momentum flux in the four quadrants (Sect. 3.1) are relatively well simulated, we can be confident in the model's ability to provide the main characteristics of turbulent structures in this particular forest.

In the stand case the well-correlated areas of u at canopy top extend mostly above the canopy, especially for quadrants II and IV that represent the dominant events for momentum transfer (Fig. 4a) and do not extend much within the trunk space. On the other hand, the well-correlated areas of w and p at canopy top (Fig. 4b, c) have a vertical elongated form extending well down into the trunk space for R_{ww} and to the ground for R_{pp}. Within the canopy (Fig. 5), where all quadrants have similar importance for momentum transfer,

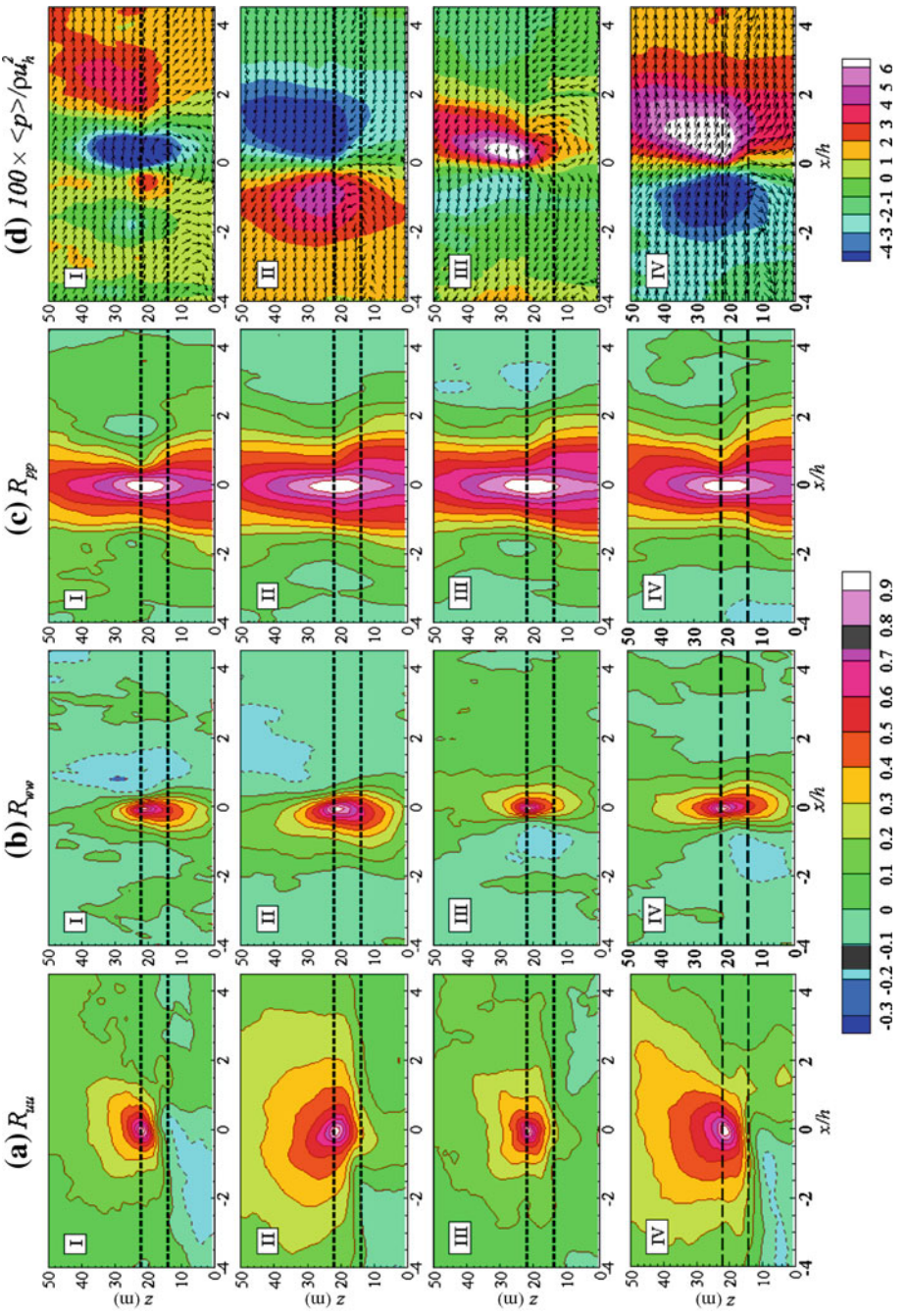

Fig. 4 Two-point autocorrelations of u (**a**), w (**b**) and p (**c**) associated with all events of each quadrant detected at the reference point. Composite averaged fields of wind-vector fluctuations and pressure perturbations, associated with all events of each quadrant (**d**). In (**d**) the *arrows* have a uniform size and only show the direction of ensemble-averaged wind-vector fluctuations. Figures from the top to the bottom refer to quadrant I to IV, respectively, corresponding in figures (**a**) to (**c**) to $R_{\phi\phi}^{\mathrm{I0}}$ to $R_{\phi\phi}^{\mathrm{IV0}}$ of Eq. 3. The figure shows the stand case, with a reference point taken at canopy top. The *dashed black lines* delimit the foliated layer of the forest

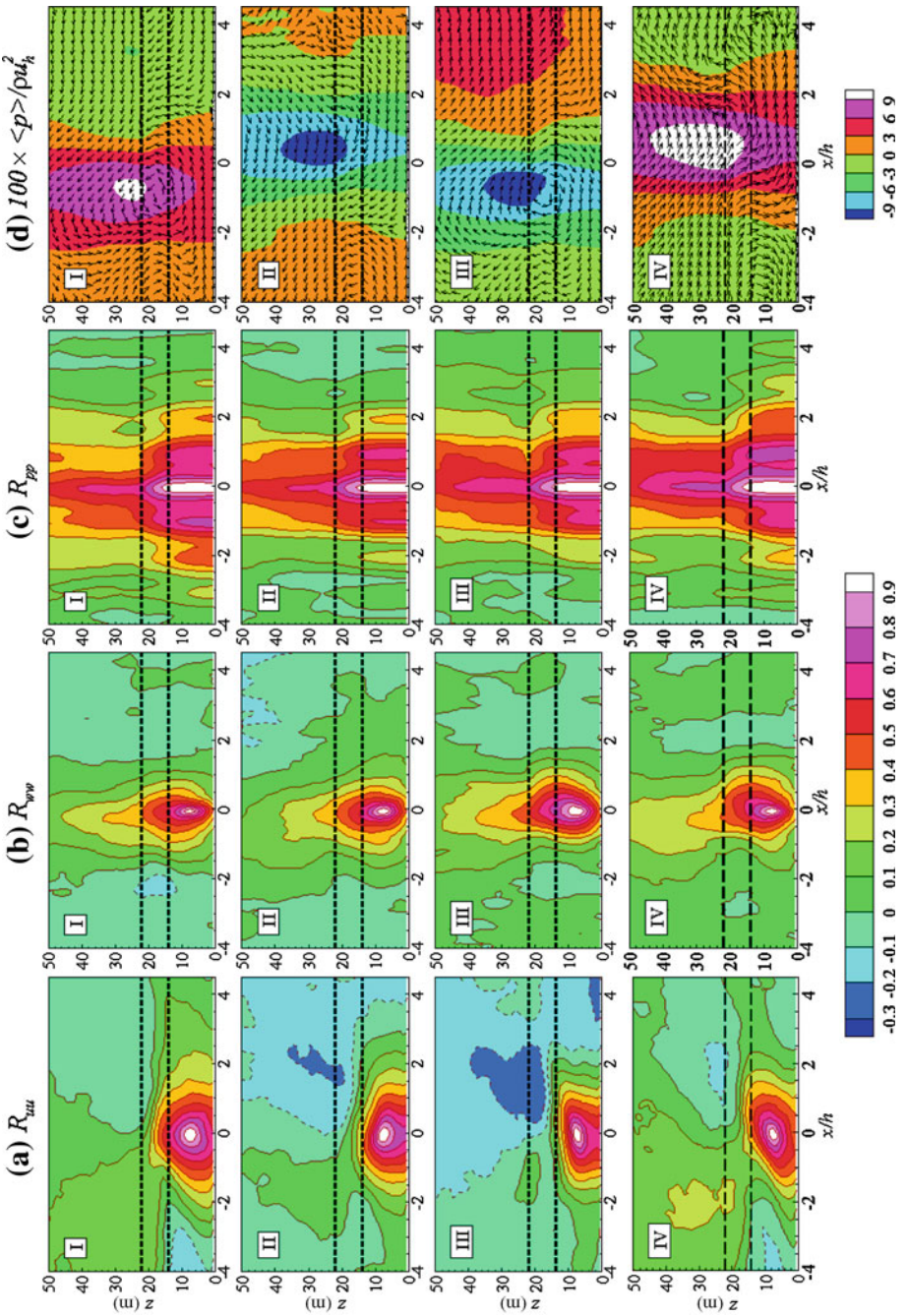

Fig. 5 Same as Fig. 4 (stand case) but with a reference point within the trunk space ($z = 0.3h$)

the correlated areas of R_{uu} are only confined within the trunk space (Fig. 5a), while those of R_{ww} and R_{pp} extend within the crown layer and above the canopy (Fig. 5b, c). The composite average of the wind-vector and pressure-perturbation fields for quadrant events at canopy top

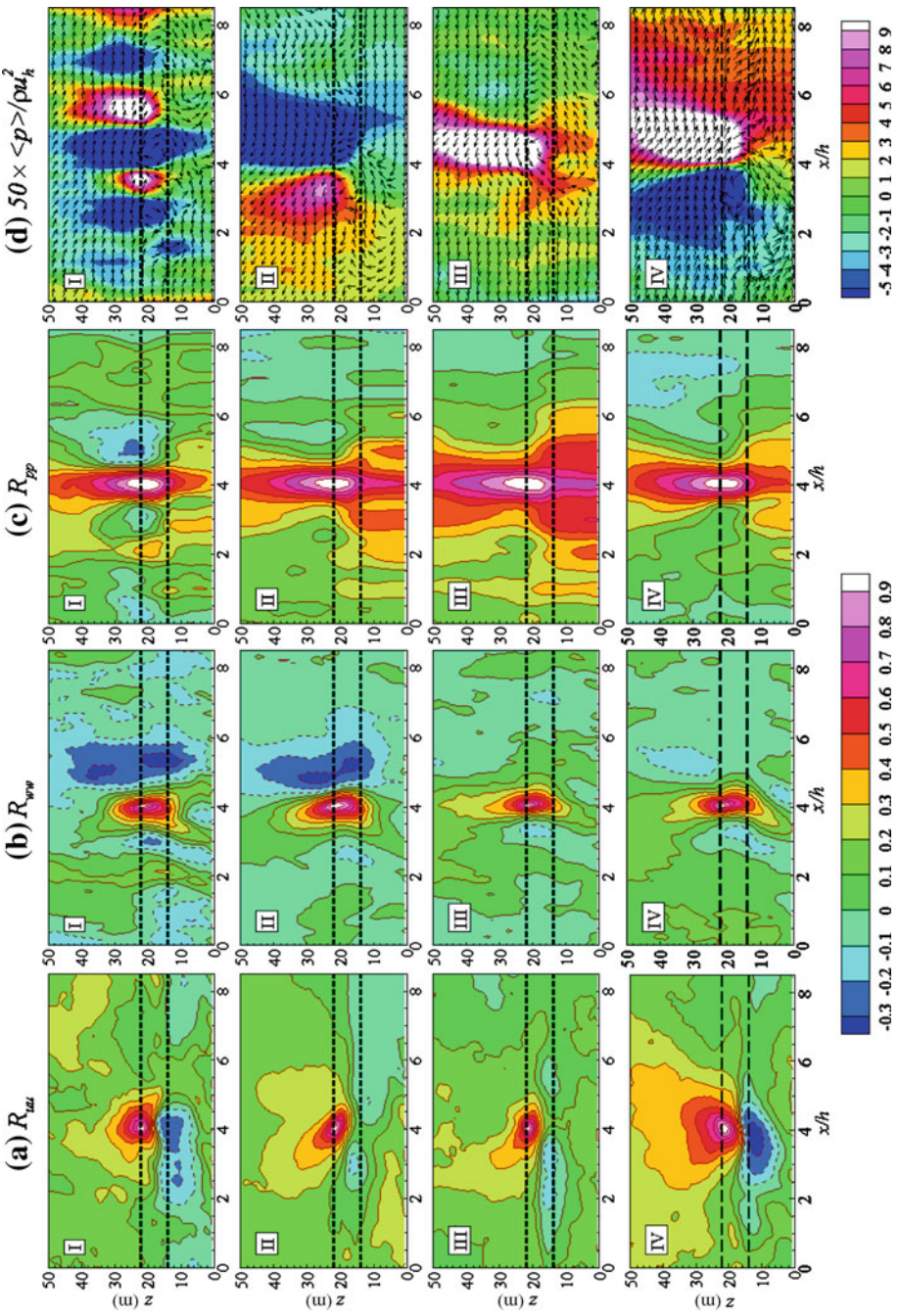

Fig. 6 Same as Fig. 4 but in the edge case, with a reference point at $x = 4h$ and $z = h$

and within the trunk space (Figs. 4d, 5d) indicate that the main momentum-flux events in the canopy are associated with a pressure effect (low-high pressure perturbations or large horizontal pressure gradient occurring at canopy top). At canopy top, sweeps and ejections

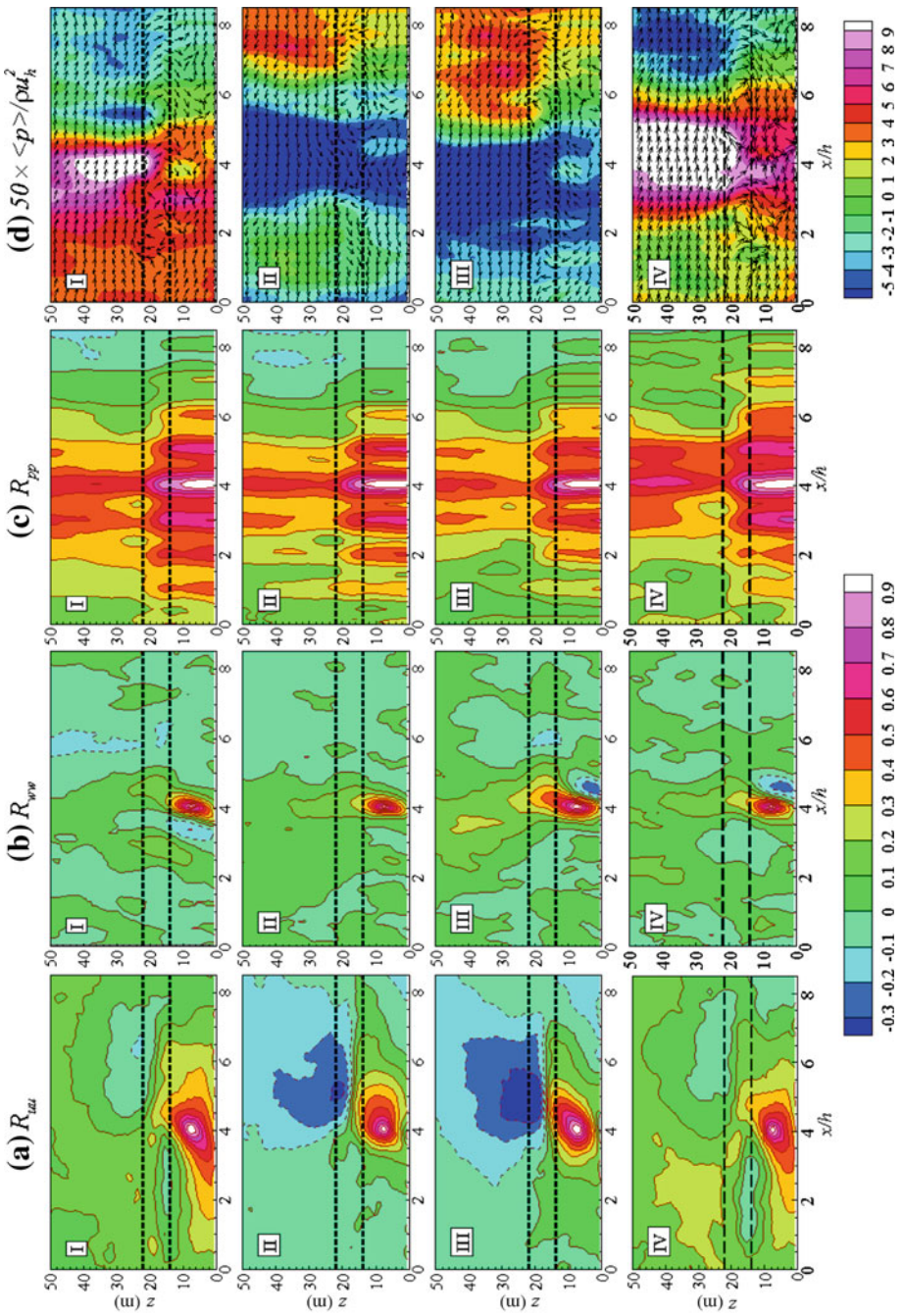

Fig. 7 Same as Fig. 4 but in the edge case and a reference point at $x = 4h$ and $z = 0.3h$

seem to be associated with downdrafts and updrafts that penetrate or come from the deep canopy, respectively (Fig. 4d). In the trunk space, events from quadrants I and III are related to counter- and clockwise rotating vortices, respectively, scaling with canopy height, and with

a core located within the crown layer (Fig. 5d). Similar vortices also seem to be associated with quadrants III and I at canopy top, respectively, but they are less frequent than sweep and ejection motions.

In the edge region at $x = 4h$ (Figs. 6, 7) the correlated areas of u, w and p are smaller than in the stand case, in all directions and at both reference points. The well-correlated areas of R_{ww} with a reference point at canopy top do not extend within the trunk space as deeply as in the stand case. Conversely the contours of R_{ww} with a reference point within the trunk space do not extend much within the crown layer. Similar behaviour is observed for R_{pp} but to a lesser extent. The composite average of the wind-vector fields does not show clear turbulent structures of canopy size as in the stand case, but only smaller structures. The smaller size of R_{uu} at canopy top may be explained by the fact that coherent eddy structures induced by the canopy are still developing in the edge region where they are confined within the growing internal boundary layer (Dupont and Brunet 2009). The size of R_{uu} may also be limited by the presence of a wind jet in the trunk space.

This spatial-correlation analysis shows that in the stand case u is well damped by the dense foliated layer while w occurs simultaneously at all levels in the canopy. The latter behaviour is certainly related to the rapid diffusion of pressure fluctuations within the canopy, as was previously observed in more uniform canopies (Raupach et al. 1989; Shaw and Zhang 1992). Because of such rapid diffusion, a clear relationship is observed between events occurring at canopy top, i.e. the development or impingement of coherent structures, and events occurring within the trunk space. Figure 8a shows the vertical variations in the convection velocity u_c, i.e. the mean velocity of the turbulent structures transported by the flow in the mean streamwise direction. It is computed from w space-time correlations simulated by the LES model in the stand case (Shaw et al. 1995). The vertical profile of u is also shown for comparison. The convection velocity appears almost constant within the canopy and equal to $1.9u_h$ (Fig. 8a), which is in good agreement with the typical value of $1.8u_h$ (Raupach et al. 1996). Such a uniform profile of u_c is usually considered as an indication that large eddies extend throughout the whole canopy depth. In the edge region, the turbulent events occurring at canopy top and within the trunk space appear less correlated than in the stand case. Turbulent structures

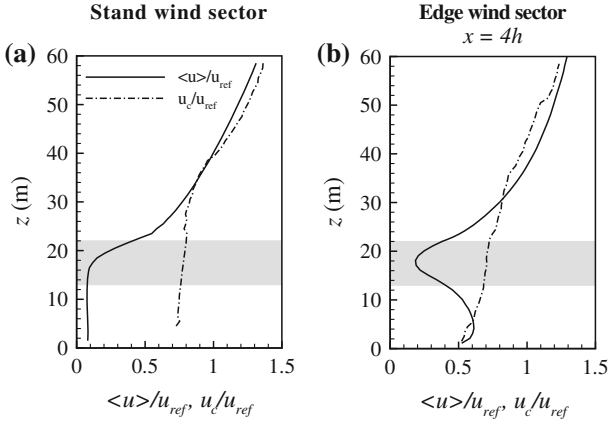

Fig. 8 Simulated vertical profiles of mean horizontal wind velocity (*solid line*) and convective velocity of turbulent structures (*dashed line*) in the stand (**a**) and edge (**b**) cases. The velocities are normalized by the reference streamwise wind velocity, u_{ref}, taken at $x = 9h$ and $z = 41.50$ m (highest level of the tower). The *shaded area* represents the crown layer

at canopy top are therefore probably different from those within the trunk space, which is confirmed by the fact that u_c is not constant in the canopy (Fig. 8b).

3.3 Measured Wind Spectra

From local point measurements, one efficient way to identify the most energetic turbulent structures is to look at wind-velocity spectra. Figure 9 shows the ensemble-averaged normalized spectra of the three velocity components recorded in the stand and edge ($x = 4$ and $9h$) wind sectors at all measurement levels. The frequency f has been normalized using the canopy height h and the mean wind velocity at canopy top, u_h, as is usually done for canopies with a uniform vertical foliage distribution. The normalization should involve typical scales of the coherent eddy structures that develop at canopy top. Kaimal and Finnigan (1994)

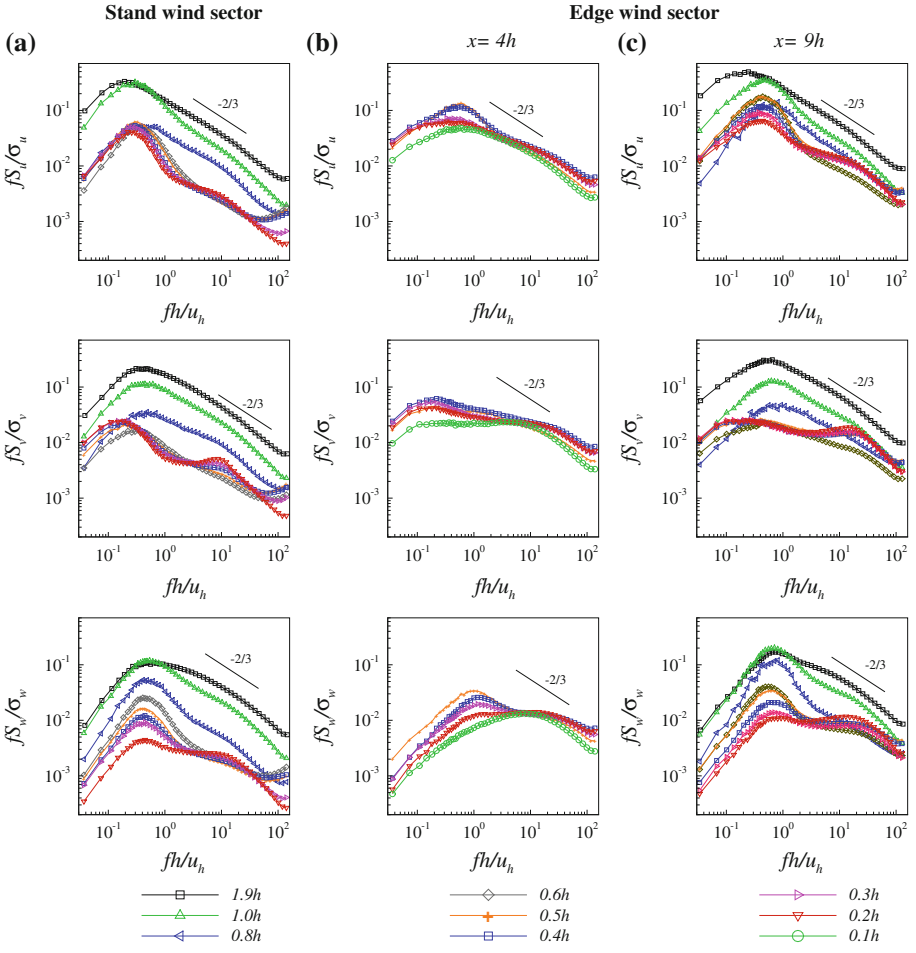

Fig. 9 Ensemble-averaged normalized energy spectra of the streamwise (*top figures*), spanwise (*middle figures*) and vertical (*bottom figures*) wind-velocity components measured from sonic anemometers at various heights within and above the forest, in the stand (**a**) and edge (**b** $x = 4h$; **c** $x = 9h$) wind sectors. The frequency f is normalized by the mean wind velocity at canopy top, u_h, and the mean canopy height, h

suggested that, for canopies with a dense crown layer and a sparse trunk space, the length scale $h - z_d$, where z_d is the canopy displacement height (=19.8 m here), may be more appropriate than h as it should scale better with coherent canopy structures. However, it follows from our two-point correlation analysis that in the stand case the correlated area of u is effectively damped within the canopy, but not that of w. In the edge case canopy eddies seem effectively smaller than h. Due to the uncertainty on finding an appropriate eddy length scale we decided to use h as the main length scale for both stand and edge cases. Regarding the velocity scale, we observed that the convection velocity of turbulent structures is constant within the canopy in the stand case and equal to $1.9u_h$, so that u_h seems to be an appropriate velocity scale there. Near the edge this is probably not true as we observed that u_c decreases within the canopy, but for the sake of simplicity we decided to retain u_h as the velocity scale.

In the stand (Fig. 9a) the wind spectra at 41.50 m display the familiar shape of atmospheric surface-layer spectra with a well-defined $-2/3$ power law in the inertial subrange. Within the canopy, from 22 to 4.5 m, a first well-defined peak is present at all levels and at the same frequency, around $fh/u_h = 0.32$ for u and 0.45 for w. The v spectra exhibit such a well-defined first peak in the upper canopy only, from 11 to 22 m, located around 0.42. The peak position of the w spectra is in agreement with the value of 0.45 (± 0.05) usually observed in canopies (Kaimal and Finnigan 1994). However the frequency of the spectral peaks for u is larger (by nearly a factor two) than the common value 0.15 (± 0.05) (Kaimal and Finnigan 1994). This discrepancy is probably related to the length scale used to normalize the frequency, which should probably be smaller than the canopy height in the present case. A better length scale may be the depth of the foliated layer, which is close to $0.41h$. Using this scale, the position of the u spectra peak becomes close to the common value, i.e. 0.13 instead of 0.15, respectively. The same scale should probably be used for v spectra but not for w spectra, as the correlated area of w does not appear damped within the canopy (see Sect. 3.2). Within the canopy the slope of all spectra appears greater in the inertial subrange region than the $-2/3$ slope, except within the crown layer for u and v. This has been observed repeatedly (Baldocchi and Meyers 1988a; Amiro 1990). Furthermore, a secondary peak is present in the inertial subrange region of the three wind-velocity spectra. It is well defined in the trunk space while only a slight bump is visible above. Close to the ground, the magnitude of this secondary maximum in the w spectra becomes very close to that of the first peak.

In the edge region ($x = 4h$ and $9h$; Fig. 9b, c) the spectral shapes are similar to those observed in the stand case, with the familiar surface-layer behaviour at 41.50 m and the presence of two peaks within the canopy. Close to the edge, at $x = 4h$, and within the trunk space, the first spectral peak is somewhat less visible than further downstream ($9h$ and stand region). These first peaks occur at the same position throughout the canopy but at a higher frequency than in the stand case, especially closer to the edge: $fh/u_h = 0.60$ and 0.45 for the u spectra at $x = 4h$ and $9h$, respectively, and $fh/u_h = 1.08$ and 0.60 for the w spectra at $x = 4h$ and $9h$ (Fig. 9b, c). Once again, this is certainly due to the length scale h being too large, and the velocity scale u_h not being proportional to the convective velocity in the edge region. The secondary peaks occur at the same frequency as in the stand case (Fig. 10b, c), except close to the edge ($x = 4h$) where its frequency appears slightly larger.

The identical position of the first spectral peak observed within the canopy in stand and edge regions confirms previous results from the autocorrelations and the convection velocity profile, that large canopy-top structures are felt within the whole canopy in stand condition. However it also contradicts other results showing that canopy-top structures at the edge may be different from those within the trunk space. The presence of a secondary peak in the inertial subrange region of the wind spectra in the canopy well

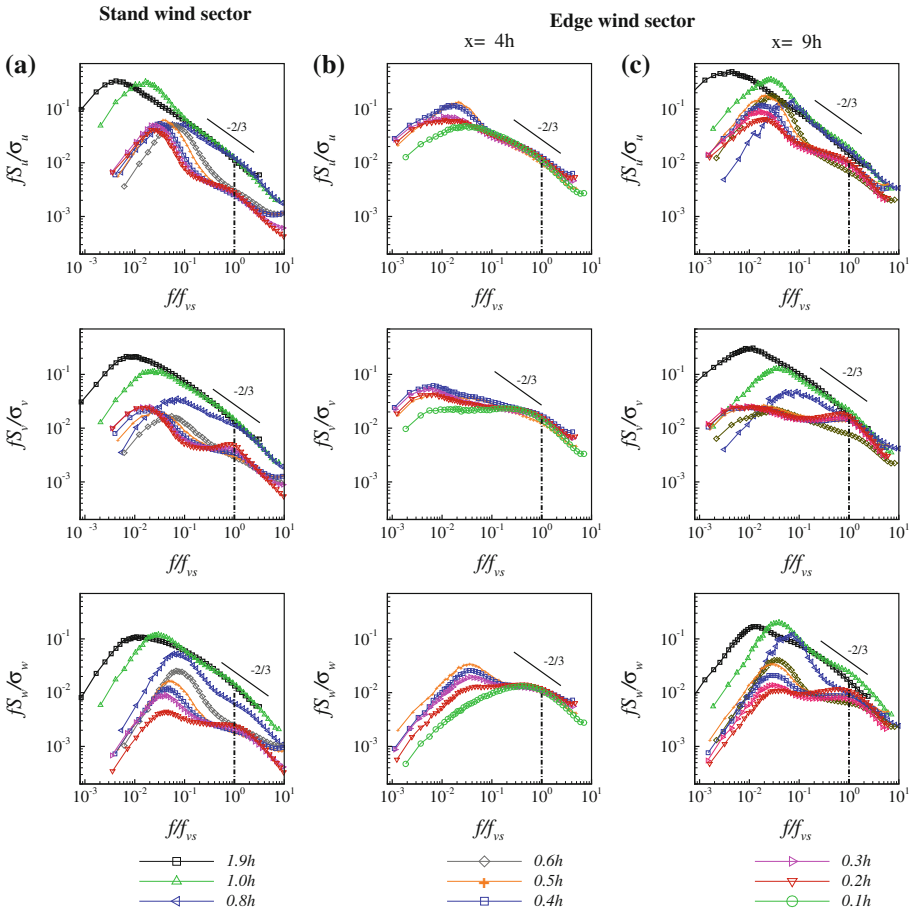

Fig. 10 Same as Fig. 9 but the frequency f is normalized by the frequency $f_{\mathrm{vs}} = 0.27\langle u\rangle/d$, of wake turbulent structures developing behind tree stems

confirms the concept of spectral short-cut suggested by Finnigan (2000). This concept implies that wake structures developing behind canopy elements should accelerate the dissipation of turbulence within the canopy and may induce a secondary spectral peak at high frequency, thereby inducing a spectral short-cut. The secondary peak observed in our case is probably related to vortex shedding behind each trunk of the canopy. If this is the case, by analogy with classical von Karman streets developing behind cylinders, the vortex frequency behind the trunks should depend on the local mean streamwise wind velocity, the stem diameter d ($= 0.33$ m here) at breast height and the Strouhal number St, such that $f_{\mathrm{vs}} = St\,\langle u\rangle\,/d$. In Fig. 10, the spectral frequency of Fig. 9 is now normalized by f_{vs} instead of u_h/h. With the optimized value $St = 0.27$, the secondary peaks then collapse remarkably well at $f/f_{\mathrm{vs}} = 1$ for all wind-velocity components. This confirms the origin of the secondary spectral peak, as was observed over an alpine hardwood forest by Cava and Katul (2008), who used a St value close to ours (0.21).

4 Discussion

The quadrant, autocorrelation and spectral analyses of turbulent structures in the present maritime pine forest have produced some complementary results, but have also revealed possible contradictions. In this section we attempt to synthesize these results into a general description of the turbulent structures present in this forest, in relation with the momentum-flux characteristics. The stand and edge cases will be considered separately.

4.1 Stand Flow

Quadrant analysis has shown that the near-zero momentum flux observed in the trunk space far from the edge results from an equilibrium between flow motions bringing and removing momentum. The autocorrelation analysis indicates that these motions are mostly related to coherent structures impinging or developing at canopy top. As the convection velocity and the position of the main peak in velocity spectra were found constant within the canopy, these structures appear to extend throughout the whole canopy depth. Although the well-correlated u area around canopy top, at zero time lag, does not extend below the crown layer, it is still possible that the structures are inclined and phase shifted within the canopy. However the fact that most of the momentum is absorbed by the crown layer reveals that the turbulent structures diffuse through pressure effects rather than explicitly penetrate the whole canopy.

One way to test this hypothesis is to investigate the origin of turbulence and momentum flux within the trunk space. To this purpose, the mean vertical profiles of all budget terms for vertical and streamwise velocity variances, $\langle w'^2 \rangle$ and $\langle u'^2 \rangle$, as defined in Eq. 5, have been calculated from the LES fields. Figure 11a shows that the $\langle w'^2 \rangle$ budget is dominated, (i) above the canopy by pressure redistribution, acting as a source, and by pressure and turbulent transport acting as a sink; (ii) within the crown layer by pressure transport (source) and drag dissipation (sink); and (iii) within the trunk space (see Fig. 11c for a magnified view) by pressure transport (source) and redistribution (sink). All other terms are smaller. Similarly, the $\langle u'^2 \rangle$ budget (Fig. 11b, d) is dominated, (i) above the canopy by shear production (source), pressure redistribution and turbulent transport (sinks); (ii) within the foliated layer by shear production and turbulent transport (sources), and pressure redistribution and drag dissipation (sinks); and (iii) within the trunk space by pressure redistribution (source), turbulent transport and drag dissipation (sinks). Consequently, the main source of vertical velocity variance within the trunk space is pressure transport from above, while its main sink is pressure redistribution towards the variances of the other two velocity components, and in particular the streamwise velocity variance for which pressure redistribution is the main source. Over a more uniform canopy, Dwyer et al. (1997) also observed from their LES that the pressure transport term dominates the TKE budget in the lowest third and the lowest two thirds of sparse and dense canopies, respectively. Regarding the origin of momentum flux within the trunk space, we showed in Dupont et al. (2011) that in this region the momentum flux is also dominated by pressure effects, and resulted from a balance between pressure strain, acting as a shear source, and pressure transport. Hence, budgets of momentum flux and TKE indicate that air motions, or more appropriately wind fluctuations within the trunk space, are more likely related to pressure fluctuations induced by canopy-top structures than by coherent structures sweeping through the whole canopy. Pressure first acts on the vertical wind velocity component, then on the horizontal components through pressure redistribution.

A consequence of such rapid pressure diffusion within the canopy is that spatial autocorrelations and velocity spectra may not be appropriate for identifying the vertical spatial scale of canopy coherent structures, because pressure may enhance the actual structure

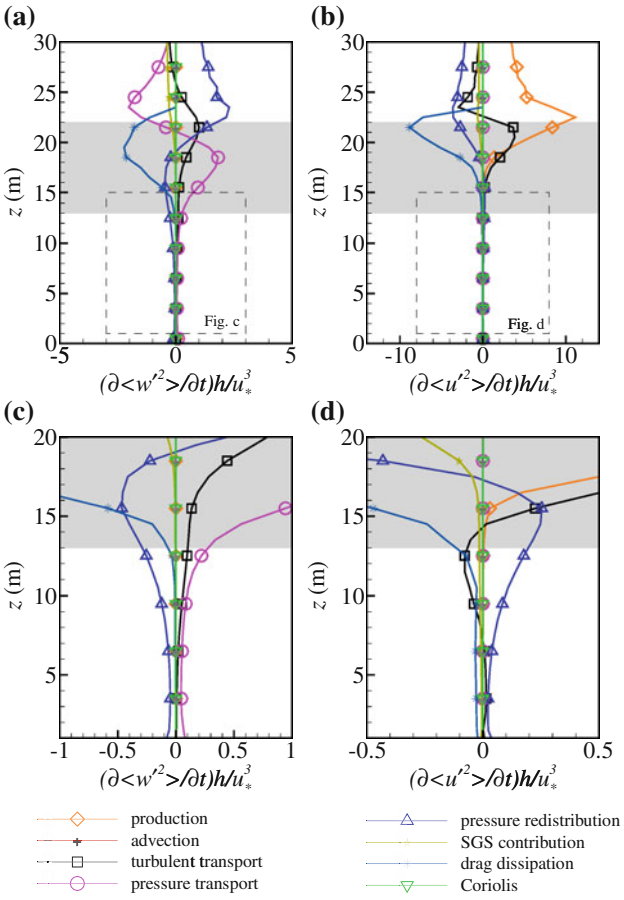

Fig. 11 Vertical profiles of the vertical $\langle w'^2 \rangle$ (**a** and **c**) and streamwise $\langle u'^2 \rangle$ (**b** and **d**) wind velocity variance budgets throughout the forest canopy in the stand case deduced from LES. Figures (**c**) and (**d**) provide an enlarged view of figures (**a**) and (**b**), respectively, in the trunk space. All budget terms are normalized by the canopy height h and the friction velocity u_*, and are defined in Eq. 5. The *shaded area* represents the crown layer

scale. This comment is particularly relevant for dense canopies where most of the momentum is absorbed by the upper canopy. Another consequence is that, qualitatively speaking, there cannot be full decoupling in momentum exchange between the upper and the lower layers of this type of canopy because of pressure diffusion; however turbulent momentum exchange remains small in magnitude.

In addition to the large-eddy structures developing at canopy top, the presence of wake structures forming behind tree stems has been deduced from the existence of secondary peaks in the inertial subrange regions of velocity spectra, in agreement with previous observation of Cava and Katul (2008) in an alpine hardwood forest. The peak frequency has been shown to be compatible with that of classical von Karman vortices, although the role of these structures in turbulent transfer within the trunk space is not clear. They should probably contribute to increasing turbulent mixing within the trunk space as well as the dissipation of larger eddy structures, bypassing the inertial eddy cascade (Finnigan 2000). Due to the

horizontal resolution of the LES model, i.e. 2 m, these wake structures are considered as SGS structures and are not explicitly simulated. They are easily identifiable from wind velocity spectra because of the sparse and open trunk space in the present case. For canopies with more developed understory it may not be so, as wake structures induced by trunks should be mixed with wake structures induced by understory elements.

4.2 Edge Flow

In the edge region turbulent structures within the trunk space appear less correlated with canopy-top structures than further downstream in the stand. This could be seen from velocity autocorrelations as well as from the convection velocity profile, which is not uniform within the canopy as in stand conditions but decreases with depth. However the main momentum-flux events within the trunk space or at canopy top still seem to be associated with low or high pressure perturbations occurring at canopy top, as in the stand case, and the main peaks of wind velocity spectra appear at the same location throughout the canopy. This apparent contradiction can be solved by assuming the presence of different, but inter-related, types of coherent structures at canopy top and within the trunk space.

In order to test this hypothesis we first consider the origin of turbulence and momentum flux within the trunk space, as was done in the previous section. The mean profiles of the $\langle u'^2 \rangle$ budget terms at $x = 4h$ (Fig. 12b, d) indicate that the main source of $\langle u'^2 \rangle$ at canopy top is due to local shear production, as was observed in stand conditions and in previous wind-tunnel and field experiments on edge flow (Morse et al. 2002). However, below the crown layer the main source is still due to local shear production, instead of pressure redistribution as in the stand case (Fig. 12b, d). The $\langle w'^2 \rangle$ budget (Fig. 12a, c) just below the crown layer is mostly dominated by pressure transport and redistribution, as in stand conditions. In the middle of the trunk space (at about 6 m) the pressure redistribution term becomes the main source, as part of the $\langle u'^2 \rangle$ production is redistributed towards $\langle w'^2 \rangle$. Note that the turbulent transport term of $\langle u'^2 \rangle$, which is larger than that of $\langle w'^2 \rangle$, exhibits a negative maximum at the lower interface of the crown layer and positive maxima within both the trunk space and the crown layer. This implies a transport of turbulence from the lower interface of the crown layer to the trunk space and possibly to the crown layer. The quantities transported here are much smaller than those at canopy top. Regarding the origin of the momentum flux, we showed in Dupont et al. (2011) that its main source in the upper trunk space is the production of mean shear caused by the sub-canopy jet induced by the airflow through the trunk space. In conclusion, in contrast to what prevails further downstream, the edge region is characterized by shear production of turbulence and an upward momentum flux below the crown layer. This local production is caused by the sub-canopy jet. In addition to canopy-top coherent structures, there is therefore the possibility for the development of coherent structures at the lower interface of the crown layer, transporting momentum from within the trunk space to the crown layer and redistributing the turbulence produced at the lower interface of the crown layer toward the trunk space and the crown layer. This feature was not observed in the simulated edge flow of Yang et al. (2006) over a forest with a more uniform vertical foliage distribution (Irvine et al. 1997).

It has been established that coherent structures at the canopy top develop in the same way as in plane mixing layers, with a mean spacing proportional to the shear length scale $L_s = \langle u(h) \rangle / (\mathrm{d}\langle u(h) \rangle / \mathrm{d}z)$ (Raupach et al. 1996). The flow at the lower interface of the crown layer also exhibits some similarity with a plane mixing-layer flow. In particular, (i) the wind-velocity profile exhibits a secondary inflexion point associated with wind shear (see Dupont et al. 2011); (ii) the uw correlation coefficient, $|r_{uw}|$, exhibits a secondary

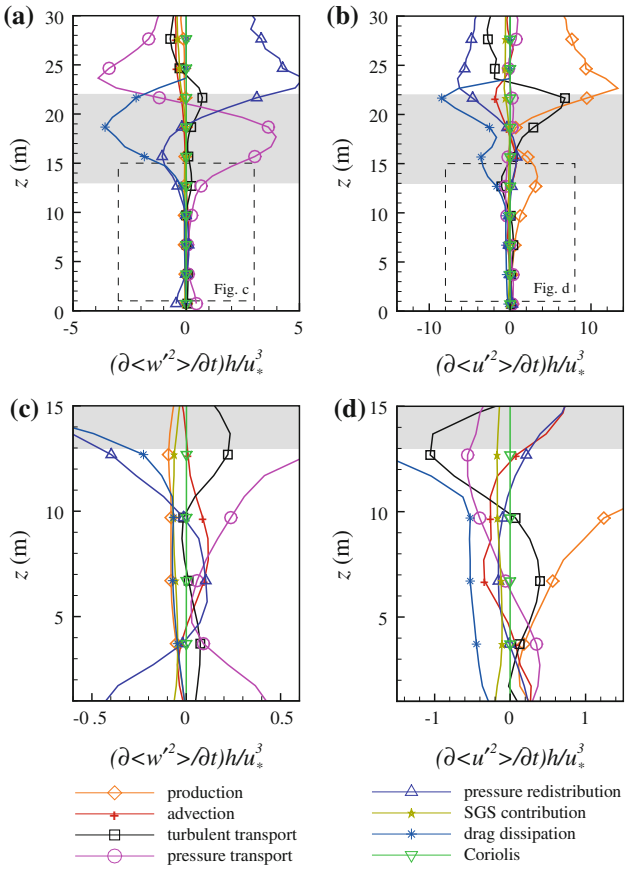

Fig. 12 Same as Fig. 11 but in the edge case ($x = 4h$)

maximum larger than 30% (figure not shown); (iii) the upward momentum flux is dominated by events from quadrants I and III, acting in the same way as sweeps and ejections for a downward momentum flux; (iv) the TKE budget is not in local equilibrium; and (v) turbulent transport exhibits a negative maximum in this region and a positive maximum in the trunk space. Consequently, the same analogy as for canopy-top structures may hold for turbulent structures developing just below the crown layer, in an 'inverted' mixing-layer configuration characterized by a slower upper flow and a faster lower flow. This secondary mixing layer is certainly not as well defined as at the canopy top since it may be perturbed by structures developing there. This may explain the absence of clear secondary maxima in the skewnesses of u and w. Furthermore, turbulent structures from this secondary mixing layer may not be as efficient as canopy-top ones since they transport much less momentum and turbulence. However they may have a similar frequency because; (i) the shear length scales L_s at both interfaces of the crown layer are close to each other ($0.23h$ at canopy top and $0.20h$ just below the crown layer), and (ii) they may be initiated by the same large-scale structures coming from well above the canopy or reaching the forest leading edge. This picture is compatible with the constancy of the main first peak of wind-velocity spectra throughout the canopy.

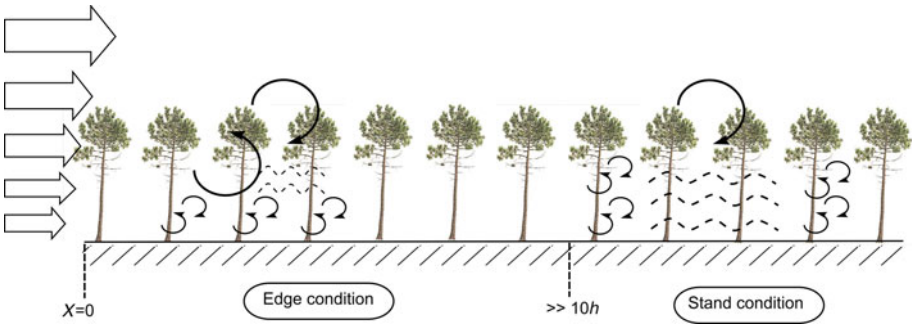

Fig. 13 Idealized representation of the main turbulent structures developing at canopy top, below the crown layer and behind tree stems, in the edge and stand of a mature maritime pine forest characterized by a deep and sparse trunk space. The waving lines within the trunk space represent pressure diffusion, as induced by canopy-top structures

5 Conclusion

In a previous study (Dupont et al. 2011) the main statistics of turbulent flow over a forest characterized by a deep and sparse trunk space were analyzed in stand and edge conditions. In the present paper, the main characteristics of turbulent structures over the same forest have been investigated, using together in situ and LES.

Different types of structures were identified within this forest canopy in both stand and edge regions; they are summarized in Fig. 13.

- The canopy-top structures developing as in plane mixing layers do not explicitly penetrate the whole canopy but rather diffuse through pressure effects, as most of their momentum is absorbed by the canopy crown layer. Hence, well within the stand turbulence in the trunk space is not directly related with canopy-top structures but with pressure fluctuations generated by them. Consequently, auto-correlation and spectral analyses are not appropriate in this case to characterize the vertical spatial scale of coherent structures since pressure diffusion enhances the actual scale of structures.
- At frequencies higher than those of canopy-top structures, wake structures developing behind tree stems are also present within the trunk space in both stand and edge. They could be identified from secondary peaks in the inertial subrange of velocity spectra. These structures may increase turbulent mixing within the trunk space as well as the dissipation of larger eddy structures, bypassing the inertial eddy cascade. The wake structures are not explicitly simulated by the LES model as they are considered as SGS structures.
- In addition to these two types of structures, mixing-layer type structures may also develop in the edge region, at the lower interface of the crown layer, under the influence of the sub-canopy wind jet induced by the airflow through the trunk space at the edge. The frequency of these structures is similar to that of canopy-top structures. They induce momentum exchange in a way similar to what occurs at canopy top, but in the opposite direction and with a lower magnitude. These structures have not been explicitly observed from measurements and LES results, but most of the conditions for their development are met; also, the upward momentum flux below the crown layer has been observed to be dominated by events from quadrants I and III, similarly to sweeps and ejections forming most of the downward momentum flux.

In conclusion, the mechanisms for biosphere–atmosphere exchanges of momentum, mass and heat may be different in forests with deep and sparse trunk space, as compared with forests characterized by a more uniform vertical foliage distribution. Two main reasons were found for this: (i) the rapid absorption of penetrating coherent structures by the crown layer, which limits exchanges between the lower canopy and the atmosphere above, (ii) the very long edge effect (greater than $10-15h$), with a strong sub-canopy wind jet that may contribute to generating local turbulent structures just below the crown layer, in addition of the turbulent structures developing at canopy top and behind tree stems.

This complex sub-canopy flow may have impacts on the micrometeorological fields within the canopy and, consequently, on sub-canopy ecosystems.

Acknowledgments We would like to thank Didier Garrigou, Sylvia Dayau, Sandra Debesa and Boris Leblanc for their contribution to the data collection and processing. We also thank the Center for Analysis and Prediction of Storms (CAPS) at the University of Oklahoma for providing the ARPS code. Computer simulations related to this work were performed using HPC resources from GENCI-IDRIS (Grant 2010-i2010011833) as well as Ephyse cluster. Thanks are expressed to the Ephyse computing team (in particular Patrick Moreau, Guy Pracros and Tovo Rabemanantsoa) for their help with the cluster set-up and administration.

Appendix: Momentum and Wind-Velocity Variance Equations

The momentum equation in ARPS is as follows:

$$\frac{\partial \widetilde{u_i}}{\partial t} = -\widetilde{u_j}\frac{\partial \widetilde{u_i}}{\partial x_j} - \frac{1}{\overline{\rho}}\frac{\partial \widetilde{p''}}{\partial x_i} - 2\omega_j\epsilon_{ijk}\widetilde{u_k} + 2\omega_j\epsilon_{ijk}U_{gk} - \frac{1}{\overline{\rho}}\frac{\partial \tau_{ij}}{\partial x_j} - C_\mathrm{d}A_\mathrm{f}V\widetilde{u_i} \qquad (4)$$

where the tilde indicates the filtered variables or grid volume-averaged variables, the overbar the base state variables and the double prime the deviation from the base state. In this equation, t is time and x_i ($x_1 = x, x_2 = y, x_3 = z$) refers to the streamwise, lateral and vertical directions, respectively; u_i ($u_1 = u, u_2 = v, u_3 = w$) is the instantaneous velocity component along x_i, V is the wind-velocity magnitude, τ_{ij} is the SGS stress tensor modelled as $-2\nu_t S_{ij}$ (where ν_t is the eddy viscosity and S_{ij} the resolved strain tensor), ϵ_{ijk} is the alternating unit tensor, p is the air pressure, ρ is the air density, and ω_i is the angular velocity of the earth projected in the u direction. The terms on the right-hand side of Eq. 4 represent, respectively, advection by the mean flow, the local pressure-gradient force, the Coriolis force, the mesoscale pressure gradient force, turbulent transport and the drag force induced by the vegetation. In the latter, C_d is the mean canopy drag coefficient and A_f is the frontal area density of the vegetation.

The budget equation for the mean resolved-scale wind velocity variance $\langle u_i' u_i' \rangle$ (Eq. 5) can be deduced from (the momentum) Eq. 4 following the procedure described in Stull (1988), and assuming neutral stratification, steady-state flow, and homogeneity in the transverse direction, viz.

$$\frac{1}{2}\frac{\partial \langle u_i' u_i' \rangle}{\partial t} = 0 = \underbrace{-\langle u_i' u_j' \rangle \frac{\partial \langle u_i \rangle}{\partial x_j}}_{\text{(I)}} \underbrace{-\frac{1}{2}\langle u_j \rangle \frac{\partial \langle u_i' u_i' \rangle}{\partial x_j}}_{\text{(II)}} \underbrace{-\frac{1}{2}\frac{\partial \langle u_j' u_i' u_i' \rangle}{\partial x_j} - \frac{\partial \langle u_i' \tau_{ij}' \rangle}{\partial x_j}}_{\text{(III)}}$$
$$\underbrace{-\frac{1}{\rho}\frac{\partial \langle u_i' p' \rangle}{\partial x_i}}_{\text{(IV)}} \underbrace{-\frac{1}{\rho}\left\langle p' \frac{\partial u_i'}{\partial x_i} \right\rangle}_{\text{(V)}} \underbrace{+\left\langle \tau_{ij}' \frac{\partial u_i'}{\partial x_j} \right\rangle}_{\text{(VI)}}$$

$$\underbrace{-C_{\mathrm{d}}A_{\mathrm{f}}\left\langle V'u_i'\right\rangle\langle u_i\rangle - C_{\mathrm{d}}A_{\mathrm{f}}\left\langle V'u_i'u_i'\right\rangle - C_{\mathrm{d}}A_{\mathrm{f}}\langle V\rangle\left\langle u_i'u_i'\right\rangle}_{\text{(VII)}}$$

$$\underbrace{-2\omega_j\epsilon_{ijk}\left\langle u_i'u_k'\right\rangle}_{\text{(VIII)}}. \tag{5}$$

The terms on the right-hand side of Eq. 5 represent, respectively, production (I), advection by the mean flow (II), transport by turbulent motion for both resolved and subgrid scales (III), pressure transport (IV), pressure redistribution (V), transfer of variance between resolved scale and subgrid scale (VI), dissipation by canopy drag (VII), and Coriolis effects (VIII).

References

Amiro B (1990) Drag coefficients and turbulence spectra within 3 boreal forest canopies. Boundary-Layer Meteorol 52(3):227–246

Baldocchi D, Meyers T (1988a) A spectral and lag-correlation analysis of turbulence in a deciduous forest canopy. Boundary-Layer Meteorol 45:31–58

Baldocchi D, Meyers T (1988b) Turbulence structure in a deciduous forest. Boundary-Layer Meteorol 43: 345–364

Black TA, Kelliher FM (1989) Processes controlling understorey evapotranspiration. Philos Trans R Soc Lond B 324(1223):207–231

Bohm M, Finnigan J, Raupach M (2000) Dispersives fluxes and canopy flows: just how important are they? In: 24th AMS conference on agricultural and forest meteorology, University of California, Davis, CA, pp 106–107

Cava D, Katul G (2008) Spectral short-circuiting and wake production within the canopy trunk space of an alpine hardwood forest. Boundary-Layer Meteorol 126:415–431

Cheng H, Castro IP (2002) Near wall flow over urban-like roughness. Boundary-Layer Meteorol 104(2):229–259

Christen A, Vogt R (2004) Direct measurement of dispersive fluxes within a cork oak plantation. In: 26th AMS conference on agricultural and forest meteorology, Vancouver, BC, Canada

Constantin J, Grelle A, Ibrom A, Morgenstern K (1999) Flux partitioning between understorey and overstorey in a boreal spruce/pine forest determined by the eddy covariance method. Agric Forest Meteorol 98(9):629–643

Dupont S, Brunet Y (2008a) Edge flow and canopy structure: a large-eddy simulation study. Boundary-Layer Meteorol 126:51–71

Dupont S, Brunet Y (2008b) Impact of forest edge shape on tree stability: a large-eddy simulation study. Forestry 81:299–315

Dupont S, Brunet Y (2008c) Influence of foliar density profile on canopy flow: a large-eddy simulation study. Agric Forest Meteorol 148:976–990

Dupont S, Brunet Y (2009) Coherent structures in canopy edge flow: a large-eddy simulation study. J Fluid Mech 630:93–128

Dupont S, Brunet Y, Finnigan JJ (2008) Large-eddy simulation of turbulent flow over a forested hill: validation and coherent structure identification. Q J Roy Meteorol Soc 134:1911–1929

Dupont S, Gosselin F, Py C, de Langre E, Hemon P, Brunet Y (2010) Modelling waving crops using large-eddy simulation: comparison with experiments and a linear stability analysis. J Fluid Mech 652:5–44

Dupont S, Bonnefond JM, Irvine MR, Lamaud E, Brunet Y (2011) Long-distance edge effects in a pine forest with a large and sparse trunk space: in situ and numerical experiments. Agric Forest Meteorol 151:328–344

Dwyer J, Patton E, Shaw R (1997) Turbulent kinetic energy budgets from a large-eddy simulation of airflow above and within a forest canopy. Boundary-Layer Meteorol 84:24–43

Finnigan J (2000) Turbulence in plant canopies. Annu Rev Fluid Mech 32:519–571

Finnigan J, Shaw R (2000) A wind-tunnel study of airflow in waving wheat: an eof analysis of the structure of the large-eddy motion. Boundary-Layer Meteorol 96(1–2):211–255

Finnigan JJ, Shaw RH, Patton EG (2009) Turbulence structure above a vegetation canopy. J Fluid Mech 637:387–424

Gao W, Shaw RH, Paw UKT (1989) Observation of organised structures in turbulent flow within and above a forest canopy. Boundary-Layer Meteorol 47:349–377
Irvine MR, Gardiner BA, Hill MK (1997) The evolution of turbulence across a forest edge. Boundary-Layer Meteorol 84(3):467–496
Kaimal JC, Finnigan JJ (1994) Atmospheric boundary layer flows. Their structure and measurements. Oxford University Press, New York, 289 pp
Klaassen W, van Breugel PB, Moors EJ, Nieveen JP (2002) Increased heat fluxes near a forest edge. Theor Appl Climatol 72(3–4):231–243
Lamaud E, Brunet Y, Berbigier P (1996) Radiation and water use efficiencies of two coniferous forest canopies. Phys Chem Earth 21:361–365
Lamaud E, Ogee J, Brunet Y, Berbigier P (2001) Validation of eddy flux measurements above the understorey of a pine forest. Agric Forest Meteorol 106(3):187–203
Lu CH, Fitzjarrald DR (1994) Seasonal and diurnal variations of coherent structures over a deciduous forest. Boundary-Layer Meteorol 69:43–69
Misson L, Baldocchi DD, Black TA, Blanken PD, Brunet Y, Yuste JC, Dorsey JR, Falk M, Granier A, Irvine MR, Jarosz N, Lamaud E, Launiainen S, Law BE, Longdoz B, Loustau D, Mckay M, Paw KT, Vesala T, Vickers D, Wilson KB, Goldstein AH (2007) Partitioning forest carbon fluxes with overstory and understory eddy-covariance measurements: a synthesis based on fluxnet data. Agric Forest Meteorol 144(1–2): 14–31
Morse AP, Gardiner BA, Marshall BJ (2002) Mechanisms controlling turbulence development across a forest edge. Boundary-Layer Meteorol 103(2):227–251
Pénelon T, Calmet I, Mironov DV (2001) Micrometeorological simulations over a complex terrain with submeso: a model study using a novel pre-processor. Int J Environ Pollut 16:583–602
Poggi D, Katul GG (2008) Micro- and macro-dispersive fluxes in canopy flows. Acta Geophys 56(3):778–799
Poggi D, Porporato A, Ridolfi L, Albertson JD, Katul GG (2004) The effect of vegetation density on canopy sub-layer turbulence. Boundary-Layer Meteorol 111(3):565–587
Raupach M, Shaw R (1982) Averaging procedures for flow within vegetation canopies. Boundary-Layer Meteorol 22:79–90
Raupach MR, Coppin PA, Legg BJ (1986) Experiments on scalar dispersion within a model-plant canopy. 1. the turbulence structure. Boundary-Layer Meteorol 35(1–2):21–52
Raupach MR, Finnigan JJ, Brunet Y (1989) Coherent eddies and turbulence in vegetation canopies. In: Fourth Australian conference on heat and mass transfer, Christchurch, NZ, pp 75–90
Raupach MR, Finnigan JJ, Brunet Y (1996) Coherent eddies and turbulence in vegetation canopies: the mixing-layer analogy. Boundary-Layer Meteorol 78(3–4):351–382
Sellier D, Brunet Y, Fourcaud T (2008) A numerical model of tree aerodynamic response to a turbulent airflow. Forestry 81(3):279–297
Shaw R, Zhang X (1992) Evidence of pressure-forced turbulent-flow in a forest. Boundary-Layer Meteorol 58(3):273–288
Shaw R, Brunet Y, Finnigan J, Raupach M (1995) A wind tunnel study of air flow in waving wheat: two-point velocity statistics. Boundary-Layer Meteorol 76(4):349–376
Sogachev A, Leclerc MY, Zhang G, Rannik U, Vesala T (2008) CO_2 fluxes near a forest edge: a numerical study. Ecol Appl 18(6):1454–1469
Stull R (1988) An introduction to boundary layer meteorology. Kluwer Academic Publishers, Dordrecht, 666 pp
Su HB, Shaw RH, Paw U KT (2000) Two-point correlation analysis of neutrally stratified flow within and above a forest from large-eddy simulation. Boundary-Layer Meteorol 94(3):423–460
Xue M, Droegemeier KK, Wong V (2000) The advanced regional prediction system (arps)—a multi-scale nonhydrostatic atmospheric simulation and prediction model. Part I: model dynamics and verification. Meteorol Atmos Phys 75(3–4):161–193
Xue M, Droegemeier KK, Wong V, Shapiro A, Brewster K, Carr F, Weber D, Liu Y, Wang D (2001) The advanced regional prediction system (arps)—a multi-scale nonhydrostatic atmospheric simulation and prediction tool. Part II: model physics and applications. Meteorol Atmos Phys 76(3–4):143–165
Yang B, Morse AP, Shaw RH, Paw U KT (2006) Large-eddy simulation of turbulent flow across a forest edge. Part ii: momentum and turbulent kinetic energy budgets. Boundary-Layer Meteorol 121(3):433–457